Chemical Physics Letters 462 (2008) 260–264

Contents lists available at ScienceDirect

Chemical Physics Letters

journal homepage: www.elsevier.com/locate/cplett

Platinum–carbon nanotube interaction

C. Bittencourt [a,*], M. Hecq [a], A. Felten [b], J.J. Pireaux [b], J. Ghijsen [b], M.P. Felicissimo [c], P. Rudolf [c], W. Drube [d], X. Ke [e], G. Van Tendeloo [e]

[a] LCIA, University of Mons-Hainaut, Bâtiment Material Nova, Parc Initialis, Av. Copernic, B-7000 Mons, Belgium
[b] LISE, University of Namur, B-5000 Namur, Belgium
[c] Zernike Institute for Advanced Materials, University of Groningen, Netherlands
[d] Deutsches Elektronen-Synchrotron DESY, D-22603 Hamburg, Germany
[e] EMAT, University of Antwerp, B-2020 Antwerp, Belgium

ARTICLE INFO

Article history:
Received 13 April 2008
In final form 23 July 2008
Available online 29 July 2008

ABSTRACT

The interaction between evaporated Pt and pristine or oxygen-plasma-treated multiwall carbon nanotubes (CNTs) is investigated. Pt is found to nucleate at defect sites, whether initially present or introduced by oxygen plasma treatment. The plasma treatment induces a uniform dispersion of Pt nanoparticles at the CNT surface. The absence of additional features in the C 1*s* core level spectrum indicates that no mixed Pt–C phase is formed. The formation of C–O–Pt bonds at the cluster-CNT interface is suggested to reduce the electronic interaction between Pt nanoparticles and the CNT surface.

1. Introduction

In 1991, Iijima reported the observation of tubular carbon structures with diameters in the order of a few nanometers thus triggering an active field of research on the properties and applications of these structures. Added to the already existing carbon family composed by graphite (2-dimensional structure), diamond (3-dimensional structure), and carbon 60 (C_{60}: spherical structure), the tubular structures named carbon nanotubes (CNTs) are considered a 1-dimensional structure [1]. Among other outstanding properties of CNTs, their well-defined geometry, exceptional mechanical properties, and extraordinary thermal and electric characteristics, qualify them for potential applications in nanoelectronic circuits, nanomechanical systems (NEMS), and catalytic systems [1–3]. Considering their application in catalytic systems, some of the most important characteristics of carbon nanotubes include their resistance to abrasion, thermal conductivity and stability and specific adsorption properties. In particular, in liquid-phase reactions they could replace activated carbons as their properties are still difficult to control and their microporosity has often slowed down the development of catalysts [3]. Table 1 compares the properties of single-wall carbon nanotubes (SWCNTs), multi-wall carbon nanotubes (MWCNTs), and activated carbon. From this, it can be seen that the broadly accepted concept that CNTs are good candidates as catalyst support due to their surface area is only partially correct, as activated carbon would be the best support in this case. Actually, the combination of mesoporosity, thermal resistance, and conductivity of CNTs should allow significant decreases on mass-transfer limitations in liquid phase reactions when compared to activated carbon, making these properties the most important characteristics of these nanostructures. In addition, carbon nanotubes are chemically stable and the higher purity of CNTs can avoid self-poisoning.

Catalytic studies performed on metal catalysts such as Pt, Ru, and Pt/Ru nanoparticles supported on CNTs have shown encouraging results in terms of activity and selectivity in a large variety of reactions [5]. In particular, high activities and selectivity have been obtained in hydrogenation reactions and electrocatalysis as compared to classical supports [3–7]. Specific metal support interactions exist that can directly affect catalytic activity and selectivity [8,9]. In general, the interaction of noble metals with the CNTs is very weak, similar to their interaction with highly oriented pyrolytic graphite (HOPG) [10]. As a result, for the optimal nanoparticle dispersion requested for high efficient in catalyst systems, the CNT surface must be homogeneously functionalized [11]. In the present study of the Pt–CNT interaction, pristine and oxygen-plasma-treated MWCNTs (f_0-CNTs) with different amounts of Pt evaporated onto their surface are analyzed.

2. Experimental

The samples were prepared using commercially available MWCNTs powder produced by chemical vapour deposition (CVD). The oxygen plasma functionalization was performed in an inductive coupled radio frequency (RF, 13.56 MHz) plasma discharge [12]. Samples for XPS and TEM analysis were simultaneously exposed to the plasma: for the XPS the MWCNT powder was supported on a copper conductive tape suitable for ultra high vacuum; the thickness and the homogeneity of the obtained

* Corresponding author.
E-mail address: carla.bittencourt@umh.ac.be (C. Bittencourt).

0009-2614/$ - see front matter © 2008 Elsevier B.V. All rights reserved.
doi:10.1016/j.cplett.2008.07.082

Table 1
Properties of CNTs (single wall carbon nanotubes SWCNTs and multi-wall carbon nanotubes MWCNTs) and activated carbon [2–4]

	Porosity ($cm^3\ g^{-1}$)	Surface area ($m^2\ g^{-1}$)	Thermal resistance in air atmosphere (°C)	Thermal conductivity (kW/m K)
SWCNT	Microporous, V_{micro}: 0.15–0.3	400–900	~800	>3
MWCNT	Mesoporous, V_{meso}: 0.5–2	200–900	~650	>3
Activated carbon	Microporous	700–1200	~500–600	$\sim 0.25 \times 10^{-3}$ up to 0.3

'CNT-layer' were checked to assure no interference of the tape on the measurements. For TEM analysis the carbon nanotubes were sonically dispersed in ethanol and a drop of the solution was deposited onto a honeycomb carbon film supported by a copper grid. The samples were treated on their support in order to avoid dispersion inside the plasma chamber and post-treatment contaminations. Once the sample was placed inside the plasma glow discharge, the treatment was performed at gas pressure of 0.1 Torr, using 15 W and the treatment time of 30 s.

Different amounts of Pt were thermally evaporated onto MWCNTs. The deposited amount was calibrated in situ by a quartz microbalance and is reported as the nominal thickness of a hypothetical continuous layer of deposited metal given in Ångstrøms (Å). Throughout this paper we will refer to the nominal thickness, as for instance the term 2 Å Pt particles, is an abbreviation for "Pt particles prepared by deposition of 2 Å Pt" and is not intended to characterize the actual size of the particles. Sample transfer from the preparation to the XPS analysis chamber was carried out while maintaining UHV conditions, the residual pressure in the analysis chamber of beam line BW2 being below 2×10^{-10} mbar.

X-ray photoemission measurements (XPS) were performed at the BW2 beamline of Hasylab using a photon energy of 3500 eV [13]. Photoelectrons were collected in normal emission geometry. The Au $4f_{7/2}$ peak at 84.0 eV recorded on a reference sample was used to calibrate the binding energy scale. In order to account for small photon energy drifts of the order of 10^{-4} eV during the measurements, Au $4f_{7/2}$ reference spectra were measured before and after recording each core level and valence band datasets.

High resolution transmission electron microscopy was performed using a Philips CM30-FEG microscope at 200 kV.

3. Results and discussion

Fig. 1 shows that Pt thermal evaporation results in the formation of clusters both at the surface of pristine and f_0-CNT. Considering that the same amount of metal was evaporated onto both samples, it can be seen that the clusters formed at the f_0-CNT surface are smaller and more uniformly dispersed. It was reported that at the graphite surface, transition-metal atoms are mobile and form clusters as the cohesive energy of these metals is much larger than the adsorption enthalpy – the nucleation is characterized by diffusion limited aggregation (DLA) [11]; nucleation centers are defects (chemical or structural) at the surface [10]. Taking into account the reported similarities between the graphite and the CNT surfaces [1], it can be assumed that Pt atoms are mobile and diffuse at the CNT-surface until they find a nucleation center. In f_0-CNT samples, it was reported that the oxygen plasma treatment grafts oxygen functional groups at the CNT surface due to O_2 dissociation on vacancies created during the plasma treatment [14]. Because Pt interacts with oxygen atoms [15], it can be suggested that in f_0-CNT the Pt nucleation centers occur in the proximity of oxygenated defects created during the treatment. Therefore, the reduction of the clusters size and their better dispersion can be associated with a higher density of well-dispersed nucleation centers created by the plasma treatment.

XPS analyses were performed in order to evaluate the chemical changes at the CNT sample due to the plasma treatment followed by the Pt evaporation. Fig. 2 shows the comparison of the XPS survey spectra recorded on CNTs before and after the oxygen plasma treatment, in addition to the XPS spectra recorded on pristine and plasma-treated Pt-decorated CNTs. The peak at 284.3 eV, observed in all spectra, is generated by photoelectrons emitted from the C 1*s* core level while the structure peaking near 530 eV in the spectrum recorded on f_0-CNT sample is due to emission from the O 1*s* core level. In addition to the peaks observed before the evaporation, spectra recorded after Pt evaporation show additional structures generated by photoelectrons emitted from Pt atoms, the more prominent ones being the 4*f* doublet components at binding energy of 74.5 eV ($4f_{5/2}$) and 71.2 eV ($4f_{7/2}$), the 4*d* doublet at 314.6 eV ($4d_{5/2}$) and 331.6 eV ($4d_{3/2}$) and the component $4p_{3/2}$ at 520 eV of the 4*p* doublet. Note that the relative intensity of the C 1*s* line in the XPS spectrum is reduced by the presence of Pt nanoparticles at the CNT surface. Due to inelastic scattering some electrons emitted from carbon atoms localized below the Pt clusters will lose part of their kinetic energy when passing through them, no longer contributing to the C 1*s* peak. The peak area ratio between the Pt 4*f* and the C 1*s* peaks for the Pt/CNT samples was found to be higher than that in the Pt/f_0-CNT samples for the same

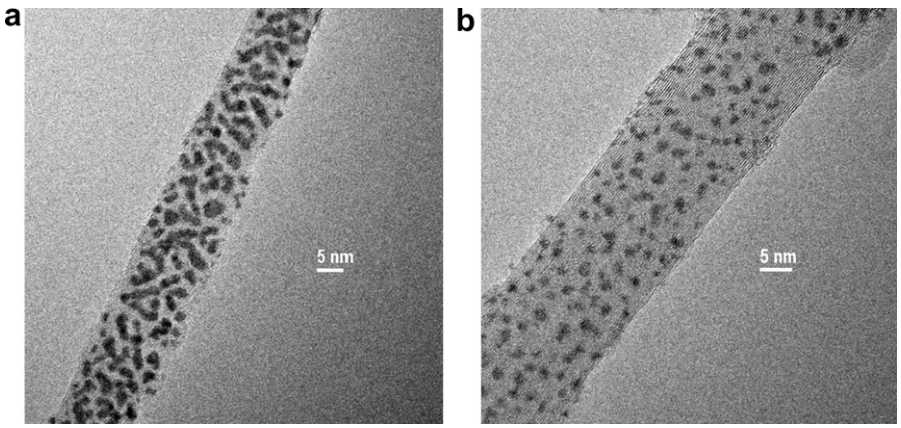

Fig. 1. TEM images of (a) pristine and (b) f_0-CNT decorated with 5 Å of Pt thermally evaporated. It can be seen that discrete particles form at the CNT-surface.

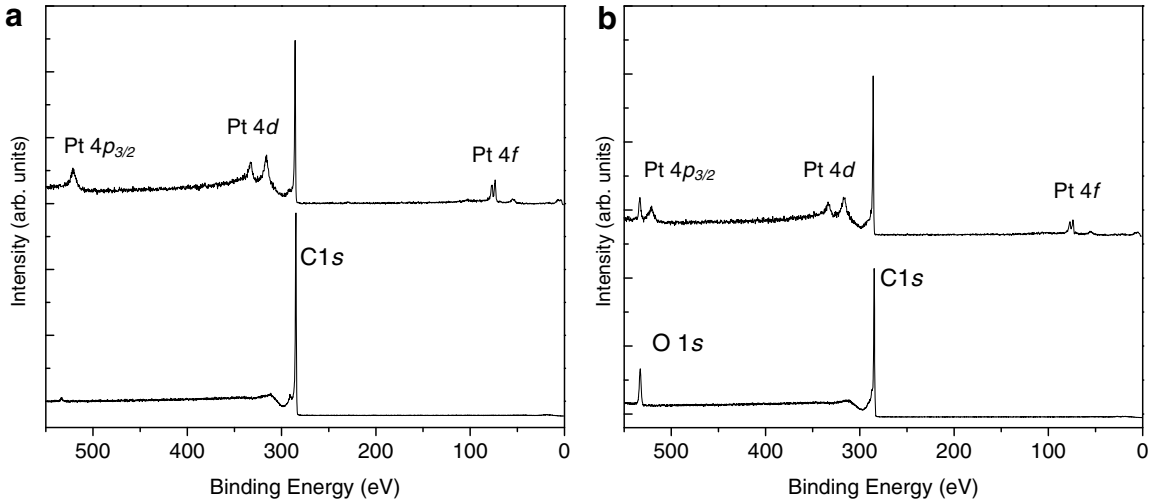

Fig. 2. Comparison of the XPS spectra recorded on (a) pristine (bottom line) and Pt coated CNTs (top line) and (b) f_0-CNTs (bottom line), and Pt coated f_0-CNTs (top line).

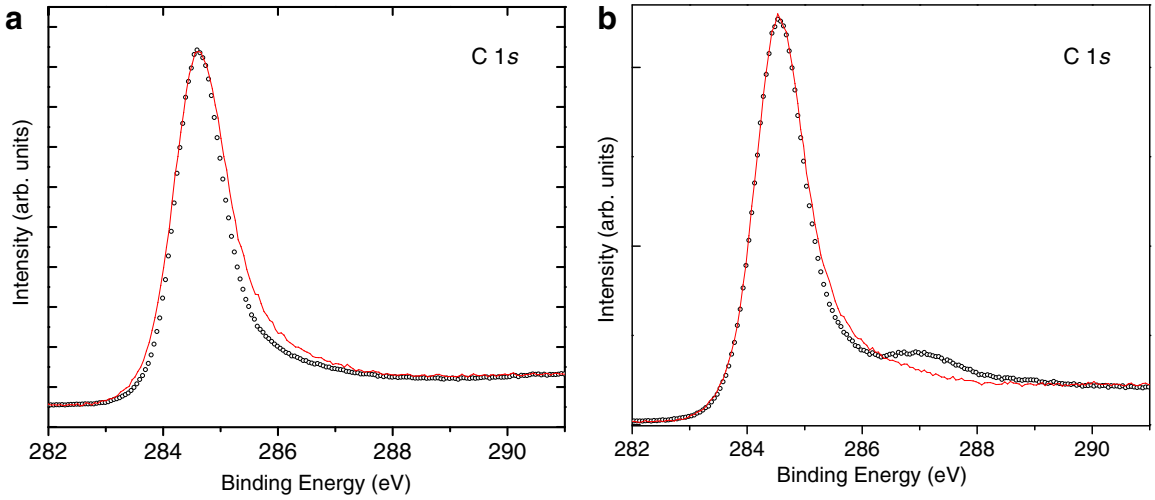

Fig. 3. Comparison of the C 1*s* spectrum recorded on (a) pristine (circle) and Pt coated CNTs (line) and (b) f_0-CNTs (circle), and Pt coated f_0-CNTs (line). The nominal amount of evaporated Pt is 10 Å.

amount of evaporated Pt, hence suggesting that the evaporation results in a denser cover of the f_0-CNTs than the pristine CNTs in agreement with the TEM results. It is important to point out that for each in situ Pt evaporation the f_0-CNT and pristine CNT samples were exposed to the same Pt beam to ensure identical coverage of both samples.

Identifying the chemical modifications produced at the CNT surface by the plasma treatment and subsequent Pt deposition is straightforward when the C 1*s* core level spectrum is analyzed. Fig. 3 shows the comparison of the C 1*s* XPS spectrum before and after the plasma treatment, the chemical modification of the CNT surface produced by the plasma treatment is revealed by the appearance of a broad structure at higher binding energy. This structure was reported to be associated with C 1*s* photoelectrons belonging to hydroxyl, carbonyl, and carboxyl (or ester) groups that were grafted at the CNT surface by the oxygen plasma treatment [12]. Inspection of the changes in the C 1*s* peak for a sequence of Pt evaporations (not shown) revealed no additional feature, indicating the absence of a mixed Pt–C phase. As no obvious change in the C 1*s* peak profile due to the evaporation of Pt onto pristine CNTs can be observed, for better comparison between the C 1*s* XPS spectra recorded before and after Pt evaporation, the spectra were superimposed. In Fig. 3, the C 1*s* peak recorded before evaporation was shifted by 0.1 eV for improving the readability, the increase in the asymmetry of the C 1*s* peak after the evaporation of 10 Å of Pt can be observed. The well-pronounced asymmetry of the C 1*s* peak recorded on graphitic-like materials reflects the high density of states (DOS) near the Fermi energy level (E_f) [16]. Hence, the increased C 1*s* peak asymmetry following the Pt deposition suggests changes in the DOS near E_f. Theoretical results have shown that when a metal atom such as Ni and Pd (which belong to the same family of the periodic table as Pt) replaces one C atom of a graphene sheet, a few electronic levels resulting from the metal atom interaction with the sheet appear close to the Fermi energy level [17,18]. This effect suggests an increase in the metallicity of this system (when compared to the graphene sheet) which explains the increase of the asymmetry in the C 1*s* peak. Moreover, the small shift to higher binding energy (~0.1 eV) of the C 1*s* peak following the Pt evaporation can be associated to an upward displacement of the Fermi energy level and consequently a rigid shift of the electronic states [16,17]. The increase in the C 1*s* peak asymmetry after the Pt evaporation is less conspicuous for the functionalized CNTs (Fig. 3b), which can be associated to the formation of C-O–Pt bonds [19] that can act as a barrier,

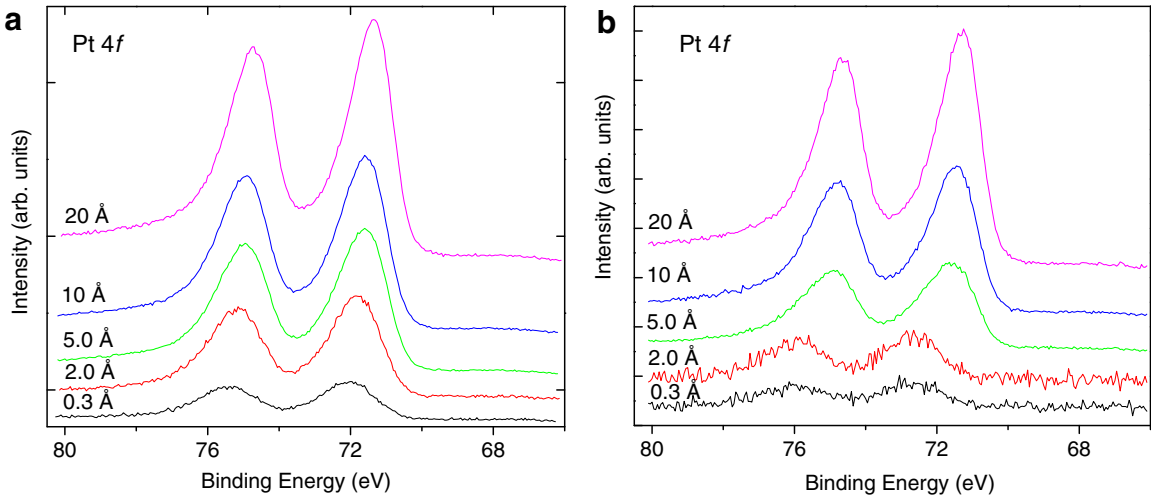

Fig. 4. Evolution of the Pt 4*f* core level for increasing amounts of nominal Pt evaporated onto pristine CNTs (a) and oxygen-plasma-treated CNTs (b).

reducing the interaction of the Pt atoms with the CNT-surface. As suggested before, photoelectrons emitted from carbon atoms below Pt clusters will lose part of their kinetic energy when passing through them, no longer contributing to the C 1*s* peak. Considering that Pt nucleation centres occur mainly in the proximity of oxygenated defects, particles forming will first cover these regions of the samples. Consequently, in the onset of the evaporation a reduction in the contribution of photoelectrons emitted from C atoms belonging to oxygen groups that are localized mainly under the cluster will show in the XPS spectrum.

The evolution of the Pt 4*f* line for a sequence of Pt evaporations onto pristine CNTs is shown in Fig 4. It can be observed that for decreasing cluster size the Pt 4*f* peaks shift towards higher binding energy and become more symmetric. For the smaller cluster, the 4*f* core levels do not exhibit the characteristic asymmetry observed for bulk metals, indicating that these clusters are not in the metallic state. The observed increase in the binding energy is largest for the smallest amount of nominal Pt evaporation, i.e., cluster size. Three factors can contribute to the core level binding energy shift: initial-state effects associated to changes in the local electronic structure (valence electron configuration), final-state effects due to changes in the relaxation process (extra-atomic response to the positively charged photohole), and cluster charging [20–24]. The influence of each of these factors on the core level binding energy depends on the nature of the cluster (i.e., the chemical composition, shape, size, and area of interaction with the support) and on the nature of the support. The experiment reveals that the Pt binding energy decreases with increasing cluster size. Such shift might possibly be explained as resulting purely from a change in the final-state relaxation, but based on the current photoemission results alone it cannot be unambiguously differentiate between initial- and final-state effects. A similar trend was observed for the clusters on oxygen-plasma-treated CNTs (Fig. 4b), the Pt 4*f* line shifts towards higher binding energy for decreasing cluster size. However, the magnitude of the energy shift cannot be compared with the shift for clusters at the pristine CNT-surface, as the higher density of nucleation sites will reduce the dimensions of the clusters (for the same amount of metal evaporated).

It is important to note that the 4*f* core-level spectrum recorded after 5 Å of deposition onto pristine CNT (Fig. 4a) exhibits a bulk-like line-shape, whilst the spectrum recorded after the deposition onto f_0-CNTs exhibits a line shape that can be decomposed by two doublets, as can be seen in Fig. 5. One is located around the binding energy position for Pt bulk (labelled as 1); the other one

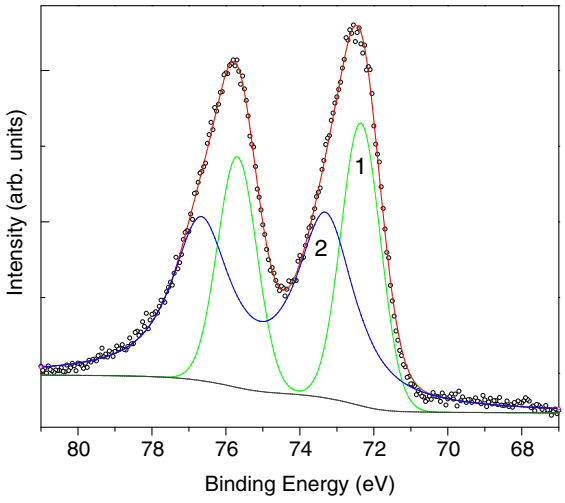

Fig. 5. Pt 4*f* core level spectrum recorded on oxygen-plasma-treated CNTs after 5 Å of Pt nominal evaporation and the result of its analysis. The doublet peak components (labelled as 1) are generated by photoelectrons emitted from Pt atoms forming metallic particles. The component labelled as 2 can be associated to photoelectrons emitted from Pt atoms in metal clusters that nucleated at oxydized defects.

is shifted to higher binding energy (labelled as 2). As the density of nucleation sites created during the oxygen plasma treatment is high, diffusion-limited aggregation cannot describe the nucleation process. Instead, the growth is influenced by nucleation taking place on oxygenated sites. The diffusion constant is therefore reduced with respect to pristine CNTs and a higher density of small particles can be found on the CNT-surface (Fig. 1). In order to interpret the origin of the doublet labelled as 2, initial- and final-state effects have to be taken into account. As mentioned before, in photoemission final-effect, the photohole left behind by the emitted photoelectron leads to a net positive charge on the cluster. The Coulomb interaction reduces the kinetic energy of the photoelectron, which therefore appears at a higher binding energy in the spectrum. This effect increases with decreasing particle diameter and is affected by the conductivity of the substrate [21]. Independent from the photoemission process, the initial-state effects are related to changes in the electronic configuration due to different chemical states (e.g., formation of Pt–O bonds) and quantum-size effects due to limited cluster dimensions. Therefore, it can be sug-

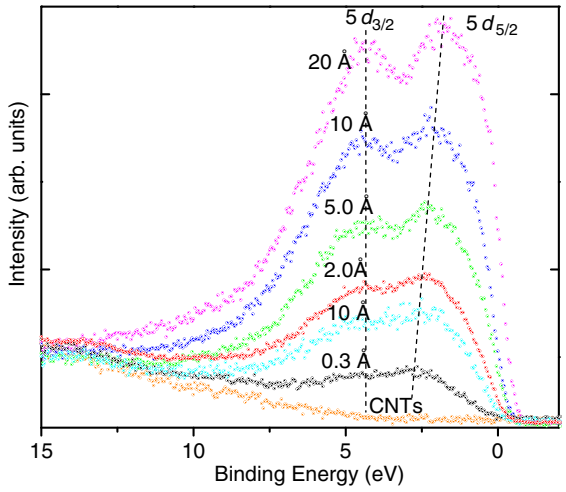

Fig. 6. Evolution of the valence band for increasing nominal amounts of Pt evaporated onto pristine CNTs.

gested that while the doublet labelled as 1 is generated by photoelectrons emitted from Pt atoms forming metallic particles, the component labelled as 2 is generated by photoelectrons emitted from Pt atoms in metal clusters that nucleated at oxidized defects forming Pt–O–C bonds at the interface.

Similar trend on the evolution of the valence band spectra for a sequence of Pt evaporations onto pristine and oxygen plasma functionalized CNTs were observed. Fig. 6 shows the development of the Pt 5*d* states with increasing cluster size; the Pt $5d_{5/2}$ level broadens as it moves towards the Fermi level while the spin-orbit splitting between the Pt $5d_{3/2}$ and $5d_{5/2}$ levels increases for increasing cluster size (Fig. 6, dashed lines). From a comparison of Figs. 4 and 5, it is observed that both the Pt 4*f* and $5d_{5/2}$ levels move toward lower binding energy for increasing cluster size. The picture emerging is the formation of metallic clusters. The growth in metallic behaviour is seen in the increasing density of states at the Fermi level as well as in the behaviour of the Pt $5d_{5/2}$ level which broadens as it moves towards the Fermi level with increasing cluster size indicating increased hybridization with the 6s electrons and a corresponding delocalization of the 5*d* electrons [25].

Based on these results, the electrostatic contribution caused by the photohole left on the cluster by the photoemission process cannot be considered negligenciable. If the neutralization of the hole is slow, on the scale of the photoemission event, there will be a shift from the bulk metal value by a Coulomb energy given by $e^2/2r$ where, r is the cluster radius. Such a contribution was stressed, for example, by Wertheim et al. for Au clusters on carbon [23].

4. Conclusion

Summarizing the results, we see the development of bulk metallic properties with increasing Pt cluster size by the shift of the 4*f* core level and the increase of its asymmetry. In addition to that, shift of the 5*d* states towards the Fermi level with increasing cluster size as well as the broadening of the 5*d* levels with increasing hybridization also account for the observed increase of the metal character of the Pt clusters. The magnitude of the Pt $4f_{7/2}$ level shift is attributed to a final state effect, i.e. to a Coulomb shift combined with atomic reconfiguration. Moreover it has been evidenced that the formation of C–O–Pt bonds at the cluster interface reduces the interaction between Pt atoms and the CNT-surface and that the oxygen plasma treatment before Pt evaporation improved significantly the cluster dispersion. The possibility to tune particles dispersion and particle-support interactions renders new insights into the catalytic properties of metal particles supported on CNTs.

Acknowledgements

This work is financially supported by the Belgian Program on Interuniversity Attraction Pole (PAI 6/08), the ARC and by DESY and the European Commission under contract RII3-CT 2004-506008 (IASFS). J.G. is research associate of NFSR, Belgium.

References

[1] R. Saito, G. Dresselhaus, M.S. Dresselhaus, Physical Properties of Carbon Nanotubes, Imperial College Press, London, 1998.
[2] L. Dong, A. Subramanian, B.J. Nelson, Nanotoday 2 (2007) 12.
[3] P. Serp, M. Corrias, P. Kalck, Appl. Catal., A: Gen. 253 (2003) 337.
[4] D. Menard, X. Py, N. Mazet, Chem. Eng. Process. 46 (2007) 565.
[5] H. Vu et al., J. Catal. 240 (2006) 18.
[6] J. Garcia, H.T. Gomes, P. Serp, P. Kalck, J.L. Figueiredo, J.L. Faria, Catal. Today 102–103 (2005) 101.
[7] H.T. Gomes, P.V. Samant, Ph. Serp, Ph. Kalck, J.L. Figueiredo, J.L. Faria, Appl. Catal., B: Environ. 54 (2004) 75.
[8] E. Weitkamp, Preparation of Solid Catalysts, Wiley-VCH, 1999.
[9] Z. Gu, P.B. Balbuena, Catal. Today 105 (2005) 152.
[10] C. Kuhrt, M. Harsdorff, Surf. Sci. 245 (1991) 173.
[11] T.A. Witten Jr., L.M. Sander, Phys. Rev. Lett. 47 (1981) 1400.
[12] A. Felten, C. Bittencourt, J.-J. Pireaux, G. Van Lier, J.C. Charlier, J. Appl. Phys. 98 (2005) 074308.
[13] W. Drube, H. Schulte-Schrepping, H.-G. Schmidt, R. Treusch, G. Materlik, Rev. Sci. Instrum. 66 (1995) 1668.
[14] R. Ionescu et al., Sens. Actuators, B: Chem. 113 (2006) 36.
[15] L.R. Saenz, P.B. Balbuena, J.M. Seminario, J. Phys. Chem. A 110 (2006) 11968.
[16] S. Hüfner, Photoelectron Spectroscopy, third edn., Springer-Verlag, Berlin, 2003. p. 173.
[17] F. Banhart, J.C. Charlier, P.M. Ajayan, Phys. Rev. Lett. 84 (2000) 686.
[18] W. Zhu, E. Kaxiras, Phys. Status Solidi B 243 (2006) 2164.
[19] K.A. Mills, R.F. Davis, S.D. Kevan, G. Thornton, D.A. Shirley, Phys. Rev. 22 (1980) 581.
[20] H.G. Boyen et al., Phys. Rev. Lett. 94 (2005) 016804.
[21] H.G. Boyen et al., Phys. Rev. B 65 (2002) 075412.
[22] V. Murgai, S. Raaen, M. Strongin, R.F. Garrett, Phys. Rev. B 33 (1986) 4345.
[23] G.K. Wertheim, S.B. DiCenzo, S.E. Youngquist, Phys. Rev. Lett. 51 (1983) 2310.
[24] W. Eberhardt, P. Fayet, D.M. Cox, Z. Fu, A. Kaldor, R. Sherwood, D. Sondericker, Phys. Rev. Lett. 64 (1990) 780.
[25] K.A. Mills, R.F. Davis, S.D. Kevan, G. Thornton, D.A. Shirley, Phys. Rev. B 22 (1980) 581.